

---

# Self-Corrected Multimodal Large Language Model for End-to-End Robot Manipulation

---

Jiaming Liu<sup>1</sup>, Chenxuan Li<sup>1\*</sup>, Guanqun Wang<sup>1\*</sup>, Lily Lee<sup>1</sup>, Kaichen Zhou<sup>1</sup>, Sixiang Chen<sup>1</sup>, Chuyan Xiong<sup>1</sup>, Jiaxin Ge<sup>1</sup>, Renrui Zhang, Shanghang Zhang<sup>1</sup> 

<sup>1</sup>National Key Laboratory for Multimedia Information Processing,  
School of Computer Science, Peking University  
{jiamingliu, 2301210279}@stu.pku.edu.cn, {wgq, shanghang}@pku.edu.cn

## Abstract


Robot manipulation policies have shown unsatisfactory action performance when confronted with novel task or object instances. Hence, the capability to automatically detect and self-correct failure action is essential for a practical robotic system. Recently, Multimodal Large Language Models (MLLMs) have shown promise in visual instruction following and demonstrated strong reasoning abilities in various tasks. To unleash general MLLMs as an end-to-end robotic agent, we introduce a Self-Corrected (SC)-MLLM, equipping our model not only to predict end-effector poses but also to autonomously recognize and correct failure actions. Specifically, we first conduct parameter-efficient fine-tuning to empower MLLM with pose prediction ability, which is reframed as a language modeling problem. When facing execution failures, our model learns to identify low-level action error causes (i.e., position and rotation errors) and adaptively seeks prompt feedback from experts. Based on the feedback, SC-MLLM rethinks the current failure scene and generates the corrected actions. Furthermore, we design a continuous policy learning method for successfully corrected samples, enhancing the model’s adaptability to the current scene configuration and reducing the frequency of expert intervention. To evaluate our SC-MLLM, we conduct extensive experiments in both simulation and real-world settings. SC-MLLM agent significantly improve manipulation accuracy compared to previous state-of-the-art robotic MLLM (ManipLLM), increasing from 57% to 79% on seen object categories and from 47% to 69% on unseen novel categories. Our project web page: <https://sites.google.com/view/sc-mlm-web>

## 1 Introduction

Recently, Multimodal Large Language Models (MLLMs) [1–7] have showcased remarkable abilities in visual instruction following and common sense reasoning. Some studies [8–11] integrate MLLMs into robot manipulation, enabling robots to explore multimodal information and formulate task plans. Concurrently, other researchers [12–15] are focusing on developing MLLMs capable of directly predicting robotic low-level action trajectories. While the integration of MLLMs into robotics has shown promising progress, the current pipelines may lead to failure predictions when faced with novel tasks or object instances. Existing methods lack the capability to automatically detect and self-correct failure actions within the closed-loop control process [16, 17]. This limitation significantly impacts their practicality in real-world settings, where uncertainties and unexpected obstacles are prevalent.

Recognizing the crucial role of self-correction in robot manipulation, recent studies have introduced some solutions. REFLECT [16] stands out by utilizing LLMs to generate failure explanations

---

\*Technical contribution,  Corresponding author.

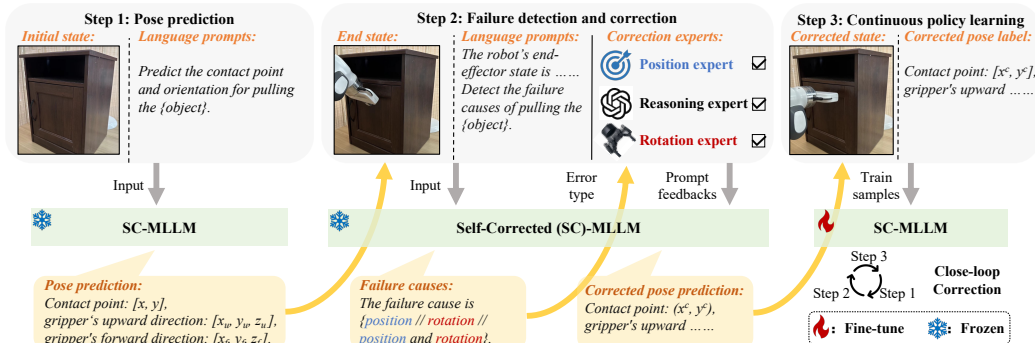


Figure 1: **Overview of our self-correction process.** **Step 1.** SC-MLLM reframes pose prediction as a language modeling problem, utilizing the initial state image and text prompts to generate the action pose. **Step 2.** SC-MLLM exploits the end-state image and end-effector parameters for failure recognition and intelligently requests prompt feedback from experts to generate corrected poses. **Step 3.** SC-MLLM continuously learns policies from successfully corrected samples, enhancing the model’s adaptability to the current scene configuration. Through correction steps, we efficiently provide a customized policy for each user, rather than relying on a shared, low-accuracy policy.

and assist a language-based planner in correcting errors. Following this innovation, subsequent researches [17–19] delve deeper into LLMs’ robot correction capabilities, correcting both high-level task planning and low-level skill primitives. However, existing robot correction methods still face two main challenges. **1) Lacking the ability to correct low-level pose prediction.** Existing methods can correct low-level skill primitives, such as generating the language prompt "Move a little bit to the right." However, these prompts are often difficult for the action model to understand and translate into specific poses. Moreover, they are unable to directly correct the pose prediction of atomic tasks, which are fundamental for completing manipulation tasks. **2) Lacking the ability to learn from correction feedback.** Current correction frameworks fail to learn from successful correction cases and improve policy predictions. They still depend on external experts (e.g., GPT-4 [20]) when encountering similar failures, which hampers their practicality and sustainable development.

In this paper, we introduce an end-to-end robotic agent called Self-Corrected (SC)-MLLM. As shown in Figure 1, SC-MLLM can directly predict end-effector poses, autonomously correct failed atomic actions, and continuously learn policies from corrected samples. To empower the pre-trained MLLM with pose prediction capability, we initially transform manipulation pose prediction into a language modeling problem, using language to directly generate poses. During the training process, we parameter-efficiently fine-tune the integrated trainable adapters [21] to preserve the inherent abilities of MLLMs. According to the static RGB image and a text prompt, our SC-MLLM generates the contact pixel coordinates on the image and an end-effector 3D direction, then projects the pixel coordinates into 3D space using depth information. To equip our model with failure detection capability, we categorize pose prediction errors as position, rotation, or combined errors, utilizing the final state image and robot end-effector pose for failure recognition. Based on the type of error, SC-MLLM dynamically requests correction feedback from experts (i.e., position [22], rotation [23], and reasoning expert [20]), leading to a reevaluation of the current failure scenario and more accurate pose predictions. Moreover, we design a continuous policy learning method tailored for successfully corrected samples, using exponential moving average techniques [24] to learn corrected poses. This method not only enhances the model’s adaptability to the current scene configuration but also reduces the frequency of expert intervention.

Note that our end-to-end SC-MLLM agent can be used multiple times within each application scenario, continuously enhancing the accuracy of our model’s pose predictions. For example, in furniture settings, the scene environment and manipulated objects differ among users. After acquiring fundamental manipulation capabilities, our SC-MLLM can undergo repeated close-loop corrections and continuous policy learning sessions within each user’s home. This process efficiently provides customized manipulation policies for each user instead of a shared low-accuracy policy.

To train our SC-MLLM, we generate 12k manipulation success samples, 15k failure samples, and corresponding 60k correction prompts in the SAPIEN simulation [25]. To systematically evaluate our method, we conduct extensive experiments in both simulation and real-world datasets. In the simulator, our method demonstrates an improvement in the manipulation success rate from 66% to

87% on seen object categories and from 30% to 68% on unseen object categories, based on expert correction prompts. After continual policy learning without expert feedback, SC-MLLM can also achieve 79% and 69% accuracy on seen and unseen categories, respectively. Additionally, we verify that SC-MLLM can correct failure cases in real-world experiments, as shown in the supplementary video. In summary, our contributions are as follows:

- To unleash general MLLMs as an end-to-end robotic agent, we introduce a Self-Corrected (SC)-MLLM, equipping our model not only to predict end-effector poses but also to autonomously recognize and correct failure actions
- Our SC-MLLM makes the first attempt to detect the failure cause of low-level pose prediction. Based on the cause, SC-MLLM can adaptively request prompt feedback from experts to rethink the current failure scene and generate the corrected action.
- We design a continuous policy learning method for corrected samples, enhancing the model’s adaptability to scene configurations and reducing expert intervention frequency.

## 2 Related work

**Robotic Manipulation.** Robotic manipulation has become a pivotal area of research due to its wide-ranging applicability. State-based reinforcement learning is a popular approach in this field [26–29]. While some studies have explored using the pure state as the policy input [27], more intricate scenarios require vision-based observation [30, 22, 31–34, 13, 35–40] to perceive the environment and comprehend complex scenes and objects [41, 42]. Besides, the Diffusion Policy [43] marks the first instance of integrating a diffusion model to learn trajectory predictions. Inspired by Multimodal Large language models’ (MLLMs) success in general scenarios [2, 1, 4, 44, 45], some works have tried to employ the common sense reasoning ability of MLLMs to solve manipulation tasks. PalmE [11] trains multimodal encodings end-to-end in conjunction with LLMs for manipulation planning. VoxPoser [34] extracts affordances and constraints from MLLMs to further zero-shot generate trajectories for manipulation tasks. RT2 [13], which transfers information to actions, holds promise for adapting more rapidly to novel situations. Robotflamingo [14] tries to fine-tune MLLM on imitation learning datasets to complete basic long-horizon tasks. ManipLLM [15] further employs the reasoning ability of MLLMs and equips it with the ability to predict end-effector poses. Although integrating MLLMs into robotics has shown promising progress, current pipelines often lead to failure predictions when facing novel tasks or object instances. Existing methods lack the capability to self-correct failed actions [46, 47] within the closed-loop control process.

**Robotic Failure Correction.** Several studies have delved into correcting robotic failures. REFLECT [16] introduces LLMs for reasoning based on a summary of past experiences, utilizing failure explanations for improved planning. MULTIREACT [19] utilizes a vision-language model [48] as a reward model to recognize and autonomously recover from intermediate execution failures. DoReMi [49] conducts immediate detection of misalignments between plans and execution using LLMs and then recovers from them. CLAIRify [50] generates iterative prompting with program verification to ensure action plans are valid. While these works demonstrate the use of LLMs in correcting execution failures in robotic tasks, they are limited to directly correcting low-level actions (e.g., 6 DoF pose) and fail to learn from the corrected feedback. In this paper, we aim to bridge this gap by allowing MLLMs to autonomously recognize and correct end-effector actions, and then continually learn from the corrected samples. Finally, due to space limitations, we include the related work on MLLMs in Appendix F.

## 3 Method

In Section 3.1, we introduce our problem formulation. Subsequently, in Section 3.2, we present our proposed Self-corrected (SC)-MLLM, detailing the model architecture design and the process of equipping our model with pose prediction and failure correction abilities. Finally, we explain the details of the continuous policy learning mechanism in Section 3.3.

### 3.1 Problem formulation

In this paper, we make the first attempt to empower the MLLM with both manipulation and failure correction abilities, constructing a closed-loop framework. Therefore, our problem formulation comprises two main components: pose prediction and action correction.

**End-effector pose prediction.** For manipulation ability, our SC-MLLM policy  $\pi$  generates an action  $a_i$  based on the image ( $I_i \in \mathbb{R}^{W \times H \times 3}$ ) and language question ( $L_i$ ) at the initial state. This action, denoted as  $\pi(I_i, L_i) \rightarrow a_i$ , corresponds to the 6-DoF control of a Franka Emika Panda robot arm [15, 31]. It is parameterized by the end-effector position and direction, where  $a_i = (a_i^{\text{pos}}, a_i^{\text{dir}})$ , with  $a_i^{\text{pos}} \in \mathbb{R}^3$  representing a 3D coordinate and  $a_i^{\text{dir}} \in \mathbb{R}^{3 \times 3}$  representing a rotation matrix. We include the end-effector position and direction in the language for MLLM fine-tuning.

**Low-level action correction.** During the actual manipulation process, robot action  $a_i$  often encounters failures, known as error action  $a_i^{\text{err}}$ . For failure correction ability, our SC-MLLM policy  $\pi$  utilize the end state RGB image ( $I_e \in \mathbb{R}^{W \times H \times 3}$ ) and the language-descriptive end-effector pose ( $L_i^{a_i}$ ) to identify failure cases, represented as  $\pi(I_e, L_i^{a_i}) \rightarrow c_i$ . Depending on the error type  $c_i$ , our SC-MLLM can dynamically request prompt feedback  $f_i$  from experts. This feedback is then utilized as input to re-predict actions  $a_c$  using our SC-MLLM policy  $\pi(I_i, f_i) \rightarrow a_c$ . Details of the correction process are provided in Section 3.2.3.

## 3.2 Self-Corrected MLLM

### 3.2.1 Model architecture

To equip our model with foundational reasoning abilities, we adopt LLaMA-Adapter V2 [51] as our base MLLM. As shown in Figure 2, when presented with an RGB image, we utilize CLIP visual encoder [48] to extract visual features. Simultaneously, text prompts are encoded into textual features using the pre-trained LLaMA tokenizer [52]. Subsequently, our MLLM employs a projection layer to align visual tokens with LLM’s token embedding, enabling the LLaMA to perform multimodal comprehension and generate corresponding answers. During the training process, we only fine-tune the injected adapters [21] within the LLM, while keeping the major pre-trained parameters frozen. This strategy is aimed at preserving the robust capabilities of the existing MLLM while enhancing the model with additional functionalities in manipulation and failure correction.

### 3.2.2 Action pose prediction

This part is aimed at enabling our SC-MLLM to generate precise end-effector poses. During the pre-collection of training data, we capture RGB images and their corresponding end-effector poses in the simulator [25] when the manipulation is successful. The collection details are described in Section 4.1. During fine-tuning, as shown in the pose prediction prompts of Figure 2 Step 1, we structure the input text prompt for pose prediction as “*Predict the contact point and orientation for pushing/pulling the object.*” The answer format is specified as “*The contact point is  $[x, y]$ , the gripper up 3D direction is  $[x_u, y_u, z_u]$ , and the gripper forward 3D direction is  $[x_f, y_f, z_f]$ .*” To simplify the direction regression prediction [15, 13], we convert it into a classification problem by discretizing the continuous numbers in the 100 normalized integer vectors into (-50, 50] discrete bins.

During inference, our SC-MLLM focuses solely on predicting the 2D coordinates  $[x, y]$  of the contact pixel on the image, which is then translated into 3D space using depth information. Meanwhile, we obtain the gripper’s left direction (gripper z-forward) from its up and forward directions based on geometric relation. To improve the accuracy of manipulation, we selectively leverage Chain-of-Thought (CoT) reasoning in real-world experiments. Specifically, we can improve the stability of the model’s pose predictions by integrating object category recognition and task planning descriptions using CoT methodology before making predictions. For example, if the model responds with “*You would typically pull the door from the right side.*” this planning-based feedback can help the model generate a more precise contact point. While CoT showcases the benefits of pose prediction, introducing it also entails additional inference time and computational costs. Therefore, we do not use this scheme in our quantitative experiment.

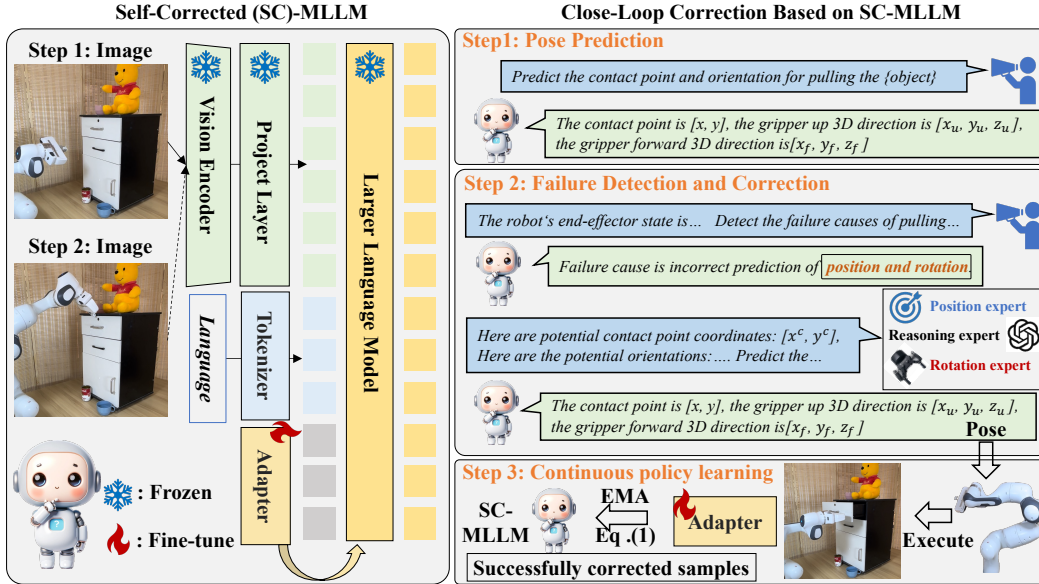


Figure 2: **Overall framework of SC-MLLM.** SC-MLLM exploit a vision encoder and projection layer to transform robot images into the LLM’s language embeddings. These embeddings are then concatenated with text tokens and fed into the LLM, which directly generates end-effector poses through language responses. **The closed-loop correction.** For self-correction, we divide the process into three steps: pose prediction, failure detection and correction, and continual policy learning. In an application scenario, we can perform multiple pipelines to enhance the manipulation stability.

### 3.2.3 Failure detection and correction

Different from previous correction works [16, 18] aimed at correcting high-level planning or low-level skill primitives, we make the first attempt to directly correct the end-effector’s 6-DoF control action. Since atomic tasks are fundamental for completing complex and long-horizon tasks, correcting the pose prediction of each atomic task is crucial. Before moving on to the correction process, it’s necessary to assess whether the action has failed and identify the causes of the failure. Specifically, we leverage our model’s inherent visual understanding capabilities, along with specific prompts, to determine whether the task has been completed. For instance, we feed the end-state image into our SC-MLLM and pose the question, “Was the microwave door closed? Please answer yes or no.” Subsequently, since the pre-trained MLLM lacks failure recognition capabilities, we fine-tune the injected adapter of our model using the failure detection prompts shown in Figure 2 Step 2. Based on the end-state image and end-effector pose, our model can accurately identify failure causes, including position, rotation, or combined errors.

Based on the error type, our SC-MLLM can adaptively request prompt feedback from specified experts and utilize this feedback to re-predict the action pose, as shown in the Figure 2 Step2. To obtain position expert prompt feedback, as shown in Figure 3 a), we first use Where2Act [22] to generate an affordance map by inputting 2D images. The affordance map indicates the probability of achieving a moving distance when operating on certain pixels, reflecting the manipulable region of objects. However, existing affordance-based methods [30, 32] can only predict a potential manipulable region with limited accuracy. For example, in Figure 3, the highest affordance score region predicted by the expert is C0-C3, which is obviously not a manipulable region. Therefore, to provide a more reliable contact point, we utilize the common sense reasoning ability of a reasoning expert (e.g., GPT-4V [20]) to further filter the contact points. Specifically, we randomly select points from areas with high affordance scores. These selected points are then projected back onto the image and fed into the reasoning expert, using the following prompt to filter: “Which of the contact points shown in the image can close the object? Please select  $n$  points ...” This process allows us to automatically obtain relatively accurate contact points, which are then used as input prompts for our SC-MLLM.

As shown in Figure 3 b), we use Anygrasp [23] to generate the rotation correction prompt. Anygrasp is trained on large-scale data and directly inputs 3D point cloud data, which includes rich contextual information, enabling accurate grasp rotation prediction. However, our actions are not limited to

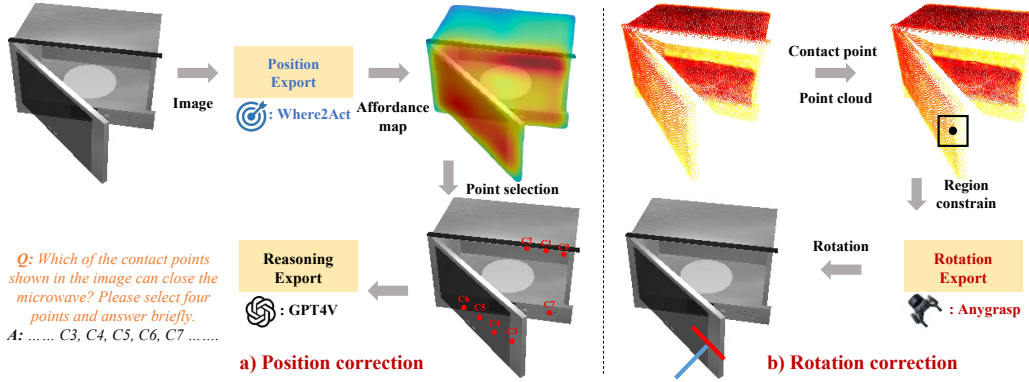


Figure 3: **The process of expert feedback.** For **position correction**, we input the end-state image into the position expert [22] to create an affordance map. Next, we randomly select points from areas with high affordance scores. These selected points are then projected back onto the image and fed into the reasoning expert [20] for potential contact point selection. For **rotation correction**, we automatically select the manipulation area (bounding box) based on the contact point predicted by our model. Subsequently, we input the point cloud into the rotation expert [23] to predict potential action rotations within the selected manipulation areas.

grasping, so we cannot predict the position and rotation for the entire object. This is why we do not use Anygrasp as the position expert. To generate the rotation for the local region of each object, we select a manipulation box based on the contact point predicted by our model and generate the rotation within the selected box region. For the manipulation box, we expand 5 pixels outward from the contact point as the center. If the failure case involves combined errors, we sequentially apply position and rotation corrections. The rotation expert uses the highest-confidence contact point provided by the position expert to generate the corresponding rotation. Finally, we combine the correction feedback for both position and rotation as input prompts for our model. To enable our SC-MLLM to understand expert feedback, we introduced a similar question format during training, as shown in the Figure 2 Step 2. During inference, our model can significantly improve the action accuracy for failure samples based on the feedback prompt, as demonstrated in Section 4.2.

### 3.3 Continuous policy learning

To empower our model with both manipulation and failure correction abilities, we integrated pose prediction, failure detection, and failure correction data for co-fine-tuning. Following previous works [4, 15], all outputs from the LLM are supervised using the cross-entropy loss  $\mathcal{L}_{ce}$ . Since the relative position of the robot and the object changes during each manipulation process, it cannot reuse previous expert feedback. Therefore, after obtaining successfully corrected samples, we design a continuous policy learning method. This method aims to enhance the pose prediction ability without requiring expert feedback prompts, as expert interventions incur additional communication costs and time. However, during fine-tuning with new successful samples, there is a risk of catastrophic forgetting, leading to a loss of capabilities in our SC-MLLM. Therefore, we explore the use of exponential moving average (EMA) [24] to continually learn from new data, formulated as:

$$\pi^t = \alpha\pi^{t-1} + (1 - \alpha)\pi^t \quad (1)$$

Where  $t$  is the time step,  $\pi$  represents our model. We set the updating weight  $\alpha = 0.999$  based on [53]. We evaluate the effectiveness of the EMA scheme in action continual learning, as shown in Appendix D. Finally, our SC-MLLM can perform repeated closed-loop corrections and continuous policy learning sessions for each scene configuration, continuously improving the model’s prediction accuracy. This process efficiently generates customized manipulation policies for each application scenario, rather than relying on a shared, low-accuracy policy.

## 4 Experiment

In this section, we conduct extensive experiments in both simulation and real-world settings. First, we introduce the experimental setup in Sec .4.1, including data collection, implementation details,

and evaluation metrics. In Sec .4.2, we compare our SC-MLLM with previous baselines on the simulation dataset. The ablation study is presented in Sec .4.3, demonstrating the effectiveness of each component. Finally, we present the qualitative analysis of real-world experiments in Sec .4.4.

#### 4.1 Experiment setting

**Data Collection.** We adopt the SAPIEN engine [25] to set up an interactive simulation environment with articulated objects from PartNet-Mobility [54]. The Franka Panda Robot, equipped with a suction gripper, serves as the robotic actuator. During data collection, we randomly select a contact point  $\mathbf{p}$  on the movable part and orient the end-effector’s z-axis opposite to its normal vector, with a random y-axis direction to interact with the object. Successful operations are categorized as successful samples and integrated into the dataset. Our training dataset comprises 12k successful manipulation samples across 20 categories. (Details are shown in Appendix B.1) For evaluation, we generate 1k examples for the test A set, comprising 20 training (seen) and 10 testing (unseen) categories. Additionally, we collect a test B set where only the relative positions between the robot and the object are altered compared to the test A set. This test B set validates the effectiveness of our continuous policy learning, ensuring it does not exhibit catastrophic forgetting or overfit to test A set.











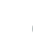




**Implementation Details.** Our SC-MLLM loads the pre-trained parameters of LLaMA-Adapter-v2 [4], which includes a pre-trained CLIP [48] as the visual encoder, a 7B LLaMA [52] model as the language model, and a multi-modal projection module consisting of 32 transformer layers. Throughout the fine-tuning phase, we utilize the Adam optimizer with  $(\beta_1, \beta_2) = (0.9, 0.999)$  and an initial learning rate of  $1e-4$ , with a warm-up period of one epoch. We fine-tuned our model on four 80G A100 GPUs for 10 epochs, with each epoch taking approximately half an hour.

**Evaluation Metric.** Follow previous works [32, 31, 15], we only test pulling accuracy in the simulator. The object starts in the closed state and the goal is to actuate the joint to its open state, *i.e.*, from near one end of its range of motion to the other end of its range. We use the predicted contact point and rotation to interact with objects in the simulator. The trajectory for pulling is predefined, moving backward along the z-axis of the end-effector. To measure the model’s performance, we employ the manipulation success rate, defined as the ratio of successfully manipulated samples to the total number of test samples. A manipulation is considered successful if the joint state difference before and after interaction exceeds a threshold of 0.1 meters. In the real-world experiment, we validate the effectiveness of our method for both pulling and pushing actions.















#### 4.2 Manipulation main results

In the main experiment, we compare our SC-MLLM against four representative baselines: UMP-Net [31], Flowbot3D [32], ManipLLM [14], and our utilized experts. Following previous SOTA work [14], we conduct comparisons with other approaches only on the initial movement setting. This reflects how well the model can generate end-effector poses for the initial state, which plays the most important role in achieving the entire long-distance movement. For a fair comparison, all methods use the same train/test split and end-effector settings. We provide the reproduction details of baselines in Appendix B.2. As shown in Table 1, by using expert feedback prompts for corrected pose prediction, Ours-c achieved an impressive 87% accuracy on seen categories and 68% accuracy on unseen categories. Compared to traditional methods, Ours-cl achieves significant improvement over UMPNet and Flowbot3D. We find that training on these diverse categories may lead to a decrease in manipulation success rates compared to the baseline original papers. This finding highlights the importance of researching MLLM-based methods, which leverage MLLM’s strong generalization capabilities to learn manipulation skills across various categories. Compared to MLLM-based methods, Ours-cl (without expert prompts) also achieved a 22% and 22% improvement on seen and unseen categories over the previous SOTA ManipLLM, respectively. The results demonstrate that our proposed method can effectively correct failed actions, learn from successfully corrected samples, and improve generalization to unseen objects. Finally, we compare SC-MLLM with our employed experts (zero-shot) to verify that the improvement does not stem from the expert prompts but also from our model’s rethinking and correction based on these prompts.

Table 1: Comparisons of our method against baseline methods. The table presents the performance of different methods across various training and test categories. "Experts" represents using our experts to zero-shot generate action poses. "Ours-p", "Ours-c", and "Ours-cl" represent our method's results for direct pose prediction, corrected prediction based on expert prompts, and continually learned policies without prompts, respectively. The representation for each category icon is shown in Table 2.

Method	Train Categories															
																
UMPNet [31]	0.23	0.36	0.41	0.22	0.24	0.30	0.43	0.34	<b>0.51</b>	0.21	0.66	0.27	0.23	0.23	0.29	0.60
FlowBot3D [32]	0.45	0.48	0.45	0.32	0.32	0.37	0.43	0.23	0.26	0.14	0.39	0.31	0.38	0.32	0.23	0.43
ManipLLM [15]	0.72	0.56	0.32	0.79	0.48	0.53	0.66	0.69	0.39	0.52	0.53	0.4	<b>0.64</b>	0.73	<b>0.62</b>	0.52
Experts	0.34	0.36	0.33	0.44	0.45	<b>0.56</b>	0.32	0.19	0.48	0.28	0.53	0.29	0.27	0.32	0.27	0.45
Ours-p	0.78	0.63	0.58	0.70	0.52	0.13	0.81	0.88	0.56	0.71	0.84	0.80	0.46	0.76	0.30	0.83
Ours-c	0.97	0.90	0.66	0.93	0.95	0.66	0.97	0.96	0.87	0.92	0.90	0.87	0.78	0.94	0.30	0.90
Ours-cl	<b>0.90</b>	<b>0.75</b>	<b>0.58</b>	<b>0.87</b>	<b>0.95</b>	0.46	<b>0.89</b>	<b>0.92</b>	0.50	<b>0.78</b>	<b>0.90</b>	<b>0.85</b>	0.63	<b>0.90</b>	0.38	<b>0.90</b>

Method	Train Categories					Test Categories											
					AVG											AVG	
UMPNet [31]	0.32	0.30	0.11	0.58	0.34	<b>0.36</b>	0.36	0.38	0.47	0.21	0.12	0.24	0.23	0.28	0.12	0.28	
FlowBot3D [32]	0.19	0.33	0.23	0.47	0.33	0.29	0.47	0.64	0.31	0.27	0.30	0.09	0.41	0.35	0.37	0.35	
ManipLLM [15]	0.39	<b>0.75</b>	0.44	0.67	0.57	0.32	0.22	0.65	<b>0.69</b>	0.38	0.85	0.27	0.53	0.26	0.38	0.47	
Experts	0.21	0.49	0.29	0.24	0.36	0.33	0.36	0.49	0.36	0.19	0.42	0.28	0.41	0.47	0.56	0.39	
Ours-p	0.20	0.68	0.48	0.60	0.66	0.09	0.25	0.39	0.66	0.64	0.23	0.21	0.56	0.10	0.50	0.30	
Ours-c	0.80	0.89	0.74	0.98	0.87	0.27	0.65	0.71	0.83	0.85	0.71	0.73	0.87	0.48	0.90	0.68	
Ours-cl	<b>0.60</b>	0.71	<b>0.74</b>	<b>0.90</b>	<b>0.79</b>	0.27	<b>0.61</b>	<b>0.71</b>	0.50	<b>0.92</b>	<b>0.69</b>	<b>0.69</b>	<b>0.80</b>	<b>0.70</b>	<b>0.81</b>	<b>0.69</b>	

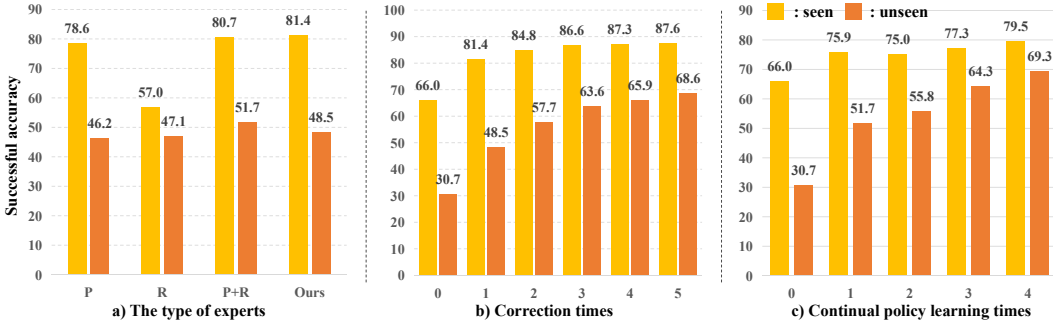


Figure 4: Ablation study for each method in our SC-MLLM framework.

### 4.3 Ablation study

To elucidate the contribution and effectiveness of individual methods within our SC-MLLM, we conduct extensive ablation studies in Figure 4.

**The impact of expert type.** First, we explore the impact of different expert feedback prompts on corrected pose prediction. As shown in Figure 4 a), "P" and "R" represent utilizing position and rotation feedback, respectively. "P + R" represents utilizing combined expert feedback, while "Ours" represents adaptively seeking expert feedback based on the failure cause. For all experiments, we input the prompt feedback into our SC-MLLM, allowing it to re-predict poses based on the prompt. We find that any type of expert prompt can improve unseen manipulation accuracy, demonstrating the importance of correction for novel object manipulation. Additionally, we observe that "Ours" achieves comparable results to "P + R", but with lower expert intervention costs. The results confirm that detecting failure cases and adaptively seeking expert feedback is essential in real-world applications. The accuracy of failure detection is shown in Appendix C.

**The impact of correction times.** Our expert system can return multiple prompts simultaneously; for example, the position expert can provide n potential contact points. Therefore, we explore the



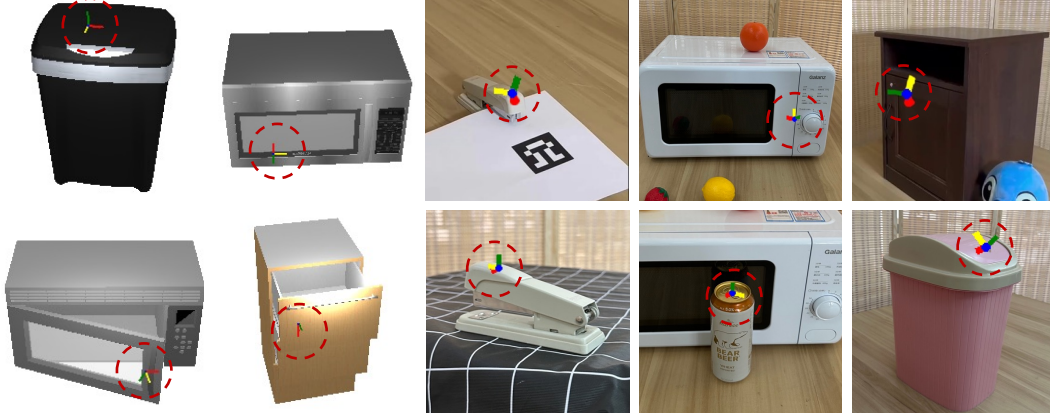


Figure 5: Visualization of pose predictions. The green, red, and yellow lines represent the z-axis, y-axis, and x-axis of the end-effector direction, while the blue dot indicates the contact point.

impact of different correction times on pose correction accuracy. As shown in Figure 4 b), the x-axis represents the number of expert prompts used for correction. Note that we count a manipulation as successful if it succeeds even once during multiple corrected actions. We find that with just one correction, the model achieves an improvement of 15.4% on seen objects and 17.8% on unseen objects compared to direct prediction without expert feedback. The results demonstrate the effectiveness of our designed correction paradigm. Furthermore, when the number of corrections reaches three or more, the model achieves a promising manipulation success rate.

**The impact of close-loop correction times** Our SC-MLLM agent can be used multiple times within each application scenario, repeating the closed-loop correction: "failure detection → failure correction → continual policy learning". As shown in Figure 4b, we aim to demonstrate whether our SC-MLLM can continually improve pose prediction accuracy without expert prompts. The x-axis represents the number of closed-loop correction iterations. We find that both seen and unseen categories show significant improvement after multiple rounds of closed-loop correction. The results not only confirm the effectiveness of our continual policy learning but also demonstrate the practicality of our method, which can efficiently provide customized manipulation policies for each user. Finally, to demonstrate that the improvements are not due to overfitting on the test A set, we also evaluate our model on the test B set after each closed-loop correction (Appendix E).

#### 4.4 Real-world evaluation

We conduct real-world experiments involving interactions with various household objects using a Franka Emika robotic arm. We modify the finger gripper by attaching double-sided tape to convert it into a suction gripper, which provides the gripper head with adhesive properties. Details are shown in the supplementary video. Although ManipLLM [15] demonstrate that MLLM-based methods are less affected by the sim-to-real domain gap, we still made efforts to increase the diversity of simulation data collection. Specifically, we increase scenario diversity by varying elements such as object part poses, camera angles, lighting, and more to mitigate the potential sim-to-real gap. As shown in Figure 5, we project our corrected pose predictions back into the 2D image using camera parameters to indicate the pose that will contact the object. The green, red, and yellow lines represent the z-axis, y-axis, and x-axis of the end-effector direction, respectively, while the blue dot indicates the contact point. After closed-loop correction, our method can accurately predict the contact point and 3D direction in the real world. In addition, for many real-world objects, our model can directly predict accurate action poses, and we only execute the correction scheme in failure cases.

### 5 Conclusion and limitation

In this paper, we innovatively propose Self-Corrected (SC)-MLLM, which can not only predict end-effector poses but also autonomously correct failure actions. Our SC-MLLM makes the first attempt to detect the failure cause of low-level pose prediction. Based on the cause, SC-MLLM can adaptively

request prompt feedback from experts to reevaluate the current failure scenario and generate the corrected action. To construct the closed-loop correction, we propose a continuous policy learning strategy that enhances the model’s adaptability and reduces the frequency of expert intervention. Through our proposed closed-loop correction, we can automatically provide customized policies for each application scenario. As for limitations, while SC-MLLM achieves promising manipulation accuracy, multiple forward propagation through the MLLM results in additional computational overhead. Our future research will focus on developing more efficient correction methods.

## References

- [1] Junnan Li, Dongxu Li, Caiming Xiong, and Steven Hoi. Blip: Bootstrapping language-image pre-training for unified vision-language understanding and generation. In *International Conference on Machine Learning*, pages 12888–12900. PMLR, 2022.
- [2] Jean-Baptiste Alayrac, Jeff Donahue, Pauline Luc, Antoine Miech, Iain Barr, Yana Hasson, Karel Lenc, Arthur Mensch, Katherine Millican, Malcolm Reynolds, et al. Flamingo: a visual language model for few-shot learning. *Advances in Neural Information Processing Systems*, 35:23716–23736, 2022.
- [3] Haotian Liu, Chunyuan Li, Qingyang Wu, and Yong Jae Lee. Visual instruction tuning. *arXiv preprint arXiv:2304.08485*, 2023.
- [4] Renrui Zhang, Jiaming Han, Aojun Zhou, Xiangfei Hu, Shilin Yan, Pan Lu, Hongsheng Li, Peng Gao, and Yu Qiao. Llama-adapter: Efficient fine-tuning of language models with zero-init attention. *arXiv preprint arXiv:2303.16199*, 2023.
- [5] Peng Gao, Renrui Zhang, Chris Liu, Longtian Qiu, Siyuan Huang, Weifeng Lin, Shitian Zhao, Shijie Geng, Ziyi Lin, Peng Jin, et al. Sphinx-x: Scaling data and parameters for a family of multi-modal large language models. *ICML 2024*, 2024.
- [6] Ziyi Lin, Chris Liu, Renrui Zhang, Peng Gao, Longtian Qiu, Han Xiao, Han Qiu, Chen Lin, Wenqi Shao, Keqin Chen, et al. Sphinx: The joint mixing of weights, tasks, and visual embeddings for multi-modal large language models. *arXiv preprint arXiv:2311.07575*, 2023.
- [7] Renrui Zhang, Dongzhi Jiang, Yichi Zhang, Haokun Lin, Ziyu Guo, Pengshuo Qiu, Aojun Zhou, Pan Lu, Kai-Wei Chang, Peng Gao, et al. Mathverse: Does your multi-modal llm truly see the diagrams in visual math problems? *arXiv preprint arXiv:2403.14624*, 2024.
- [8] Ishika Singh, Valts Blukis, Arsalan Mousavian, Ankit Goyal, Danfei Xu, Jonathan Tremblay, Dieter Fox, Jesse Thomason, and Animesh Garg. Progprompt: Generating situated robot task plans using large language models. In *2023 IEEE International Conference on Robotics and Automation (ICRA)*, pages 11523–11530. IEEE, 2023.
- [9] Michael Ahn, Anthony Brohan, Noah Brown, Yevgen Chebotar, Omar Cortes, Byron David, Chelsea Finn, Chuyuan Fu, Keerthana Gopalakrishnan, Karol Hausman, et al. Do as i can, not as i say: Grounding language in robotic affordances. *arXiv preprint arXiv:2204.01691*, 2022.
- [10] Jacky Liang, Wenlong Huang, Fei Xia, Peng Xu, Karol Hausman, Brian Ichter, Pete Florence, and Andy Zeng. Code as policies: Language model programs for embodied control. In *2023 IEEE International Conference on Robotics and Automation (ICRA)*, pages 9493–9500. IEEE, 2023.
- [11] Danny Driess, Fei Xia, Mehdi SM Sajjadi, Corey Lynch, Aakanksha Chowdhery, Brian Ichter, Ayzaan Wahid, Jonathan Tompson, Quan Vuong, Tianhe Yu, et al. Palm-e: An embodied multimodal language model. *arXiv preprint arXiv:2303.03378*, 2023.
- [12] Anthony Brohan, Noah Brown, Justice Carbajal, Yevgen Chebotar, Joseph Dabis, Chelsea Finn, Keerthana Gopalakrishnan, Karol Hausman, Alex Herzog, Jasmine Hsu, et al. Rt-1: Robotics transformer for real-world control at scale. *arXiv preprint arXiv:2212.06817*, 2022.
- [13] Brianna Zitkovich, Tianhe Yu, Sichun Xu, Peng Xu, Ted Xiao, Fei Xia, Jialin Wu, Paul Wohlhart, Stefan Welker, Ayzaan Wahid, et al. Rt-2: Vision-language-action models transfer web knowledge to robotic control. In *7th Annual Conference on Robot Learning*, 2023.

- [14] Xinghang Li, Minghuan Liu, Hanbo Zhang, Cunjun Yu, Jie Xu, Hongtao Wu, Chilam Cheang, Ya Jing, Weinan Zhang, Huaping Liu, et al. Vision-language foundation models as effective robot imitators. *arXiv preprint arXiv:2311.01378*, 2023.
- [15] Xiaoqi Li, Mingxu Zhang, Yiran Geng, Haoran Geng, Yuxing Long, Yan Shen, Renrui Zhang, Jiaming Liu, and Hao Dong. Manipllm: Embodied multimodal large language model for object-centric robotic manipulation. *arXiv preprint arXiv:2312.16217*, 2023.
- [16] Zeyi Liu, Arpit Bahety, and Shuran Song. Reflect: Summarizing robot experiences for failure explanation and correction. *arXiv preprint arXiv:2306.15724*, 2023.
- [17] Lihan Zha, Yuchen Cui, Li-Heng Lin, Minae Kwon, Montserrat Gonzalez Arenas, Andy Zeng, Fei Xia, and Dorsa Sadigh. Distilling and retrieving generalizable knowledge for robot manipulation via language corrections. *arXiv preprint arXiv:2311.10678*, 2023.
- [18] Chenlin Ming, Jiacheng Lin, Pangkit Fong, Han Wang, Xiaoming Duan, and Jianping He. Hicrisp: A hierarchical closed-loop robotic intelligent self-correction planner. *arXiv preprint arXiv:2309.12089*, 2023.
- [19] Zhouliang Yu, Jie Fu, Yao Mu, Chenguang Wang, Lin Shao, and Yaodong Yang. Multireact: Multimodal tools augmented reasoning-acting traces for embodied agent planning. 2023.
- [20] Josh Achiam, Steven Adler, Sandhini Agarwal, Lama Ahmad, Ilge Akkaya, Florencia Leoni Aleman, Diogo Almeida, Janko Altenschmidt, Sam Altman, Shyamal Anadkat, et al. Gpt-4 technical report. *arXiv preprint arXiv:2303.08774*, 2023.
- [21] Edward J Hu, Yelong Shen, Phillip Wallis, Zeyuan Allen-Zhu, Yuanzhi Li, Shean Wang, Lu Wang, and Weizhu Chen. Lora: Low-rank adaptation of large language models. *arXiv preprint arXiv:2106.09685*, 2021.
- [22] Kaichun Mo, Leonidas J Guibas, Mustafa Mukadam, Abhinav Gupta, and Shubham Tulsiani. Where2act: From pixels to actions for articulated 3d objects. In *Proceedings of the IEEE/CVF International Conference on Computer Vision*, pages 6813–6823, 2021.
- [23] Hao-Shu Fang, Chenxi Wang, Hongjie Fang, Minghao Gou, Jirong Liu, Hengxu Yan, Wenhai Liu, Yichen Xie, and Cewu Lu. Anygrasp: Robust and efficient grasp perception in spatial and temporal domains. *IEEE Transactions on Robotics*, 2023.
- [24] Antti Tarvainen and Harri Valpola. Mean teachers are better role models: Weight-averaged consistency targets improve semi-supervised deep learning results. *Advances in neural information processing systems*, 30, 2017.
- [25] Fanbo Xiang, Yuzhe Qin, Kaichun Mo, Yikuan Xia, Hao Zhu, Fangchen Liu, Minghua Liu, Hanxiao Jiang, Yifu Yuan, He Wang, Li Yi, Angel X. Chang, Leonidas J. Guibas, and Hao Su. SAPIEN: A simulated part-based interactive environment. In *The IEEE Conference on Computer Vision and Pattern Recognition (CVPR)*, June 2020.
- [26] Shirin Joshi, Sulabh Kumra, and Ferat Sahin. Robotic grasping using deep reinforcement learning. In *2020 IEEE 16th International Conference on Automation Science and Engineering (CASE)*, pages 1461–1466. IEEE, 2020.
- [27] OpenAI: Marcin Andrychowicz, Bowen Baker, Maciek Chociej, Rafal Jozefowicz, Bob McGrew, Jakub Pachocki, Arthur Petron, Matthias Plappert, Glenn Powell, Alex Ray, et al. Learning dexterous in-hand manipulation. *The International Journal of Robotics Research*, 39(1):3–20, 2020.
- [28] Denis Yarats, Rob Fergus, Alessandro Lazaric, and Lerrel Pinto. Mastering visual continuous control: Improved data-augmented reinforcement learning. *arXiv preprint arXiv:2107.09645*, 2021.
- [29] Yiran Geng, Boshi An, Haoran Geng, Yuanpei Chen, Yaodong Yang, and Hao Dong. End-to-end affordance learning for robotic manipulation. In *International Conference on Robotics and Automation (ICRA)*, 2023.

- [30] Kaichun Mo, Shilin Zhu, Angel X. Chang, Li Yi, Subarna Tripathi, Leonidas J. Guibas, and Hao Su. PartNet: A large-scale benchmark for fine-grained and hierarchical part-level 3D object understanding. In *The IEEE Conference on Computer Vision and Pattern Recognition (CVPR)*, June 2019.
- [31] Zhenjia Xu, Zhanpeng He, and Shuran Song. Universal manipulation policy network for articulated objects. *IEEE Robotics and Automation Letters*, 7(2):2447–2454, 2022.
- [32] Ben Eisner, Harry Zhang, and David Held. Flowbot3d: Learning 3d articulation flow to manipulate articulated objects. *arXiv preprint arXiv:2205.04382*, 2022.
- [33] Ruihai Wu, Yan Zhao, Kaichun Mo, Zizheng Guo, Yian Wang, Tianhao Wu, Qingnan Fan, Xuelin Chen, Leonidas Guibas, and Hao Dong. Vat-mart: Learning visual action trajectory proposals for manipulating 3d articulated objects. *arXiv preprint arXiv:2106.14440*, 2021.
- [34] Wenlong Huang, Chen Wang, Ruohan Zhang, Yunzhu Li, Jiajun Wu, and Li Fei-Fei. Voxposer: Composable 3d value maps for robotic manipulation with language models. *arXiv preprint arXiv:2307.05973*, 2023.
- [35] Yinzhen Xu, Weikang Wan, Jialiang Zhang, Haoran Liu, Zikang Shan, Hao Shen, Ruicheng Wang, Haoran Geng, Yijia Weng, Jiayi Chen, et al. Unidexgrasp: Universal robotic dexterous grasping via learning diverse proposal generation and goal-conditioned policy. *arXiv preprint arXiv:2303.00938*, 2023.
- [36] Weikang Wan, Haoran Geng, Yun Liu, Zikang Shan, Yaodong Yang, Li Yi, and He Wang. Unidexgrasp++: Improving dexterous grasping policy learning via geometry-aware curriculum and iterative generalist-specialist learning. *arXiv preprint arXiv:2304.00464*, 2023.
- [37] Ran Gong, Jiangyong Huang, Yizhou Zhao, Haoran Geng, Xiaofeng Gao, Qingyang Wu, Wensi Ai, Ziheng Zhou, Demetri Terzopoulos, Song-Chun Zhu, Baoxiong Jia, and Siyuan Huang. Arnold: A benchmark for language-grounded task learning with continuous states in realistic 3d scenes. *arXiv preprint arXiv:2304.04321*, 2023.
- [38] Jingyun Yang, Congyue Deng, Jimmy Wu, Rika Antonova, Leonidas Guibas, and Jeannette Bohg. Equivact: Sim(3)-equivariant visuomotor policies beyond rigid object manipulation. *arXiv preprint arXiv:2310.16050*, 2023.
- [39] Qianxu Wang, Haotong Zhang, Congyue Deng, Yang You, Hao Dong, Yixin Zhu, and Leonidas Guibas. Sparsedff: Sparse-view feature distillation for one-shot dexterous manipulation. *arXiv preprint arXiv:2310.16838*, 2023.
- [40] Haoran Geng, Songlin Wei, Congyue Deng, Bokui Shen, He Wang, and Leonidas Guibas. Sage: Bridging semantic and actionable parts for generalizable articulated-object manipulation under language instructions. *arXiv preprint arXiv:2312.01307*, 2023.
- [41] Congyue Deng, Jiahui Lei, Bokui Shen, Kostas Daniilidis, and Leonidas Guibas. Banana: Banach fixed-point network for pointcloud segmentation with inter-part equivariance. *arXiv preprint arXiv:2305.16314*, 2023.
- [42] Jiahui Lei, Congyue Deng, Bokui Shen, Leonidas Guibas, and Kostas Daniilidis. Nap: Neural 3d articulation prior. *arXiv preprint arXiv:2305.16315*, 2023.
- [43] Cheng Chi, Siyuan Feng, Yilun Du, Zhenjia Xu, Eric Cousineau, Benjamin Burchfiel, and Shuran Song. Diffusion policy: Visuomotor policy learning via action diffusion. *arXiv preprint arXiv:2303.04137*, 2023.
- [44] Ziyu Guo, Renrui Zhang, Xiangyang Zhu, Yiwen Tang, Xianzheng Ma, Jiaming Han, Kexin Chen, Peng Gao, Xianzhi Li, Hongsheng Li, et al. Point-bind & point-llm: Aligning point cloud with multi-modality for 3d understanding, generation, and instruction following. *arXiv preprint arXiv:2309.00615*, 2023.
- [45] Bo Li, Kaichen Zhang, Hao Zhang, Dong Guo, Renrui Zhang, Feng Li, Yuanhan Zhang, Ziwei Liu, and Chunyuan Li. Llava-next: Stronger llms supercharge multimodal capabilities in the wild, May 2024.

- [46] Zhibin Gou, Zhihong Shao, Yeyun Gong, Yelong Shen, Yujiu Yang, Nan Duan, and Weizhu Chen. Critic: Large language models can self-correct with tool-interactive critiquing. *arXiv preprint arXiv:2305.11738*, 2023.
- [47] Jiaxin Ge, Sanjay Subramanian, Trevor Darrell, and Boyi Li. From wrong to right: A recursive approach towards vision-language explanation. *arXiv preprint arXiv:2311.12391*, 2023.
- [48] Alec Radford, Jong Wook Kim, Chris Hallacy, Aditya Ramesh, Gabriel Goh, Sandhini Agarwal, Girish Sastry, Amanda Askell, Pamela Mishkin, Jack Clark, et al. Learning transferable visual models from natural language supervision. In *International conference on machine learning*, pages 8748–8763. PMLR, 2021.
- [49] Yanjiang Guo, Yen-Jen Wang, Lihan Zha, Zheyuan Jiang, and Jianyu Chen. Doremi: Grounding language model by detecting and recovering from plan-execution misalignment. *arXiv preprint arXiv:2307.00329*, 2023.
- [50] Marta Skreta, Naruki Yoshikawa, Sebastian Arellano-Rubach, Zhi Ji, Lasse Bjørn Kristensen, Kourosh Darvish, Alán Aspuru-Guzik, Florian Shkurti, and Animesh Garg. Errors are useful prompts: Instruction guided task programming with verifier-assisted iterative prompting. *arXiv preprint arXiv:2303.14100*, 2023.
- [51] Peng Gao, Jiaming Han, Renrui Zhang, Ziyi Lin, Shijie Geng, Aojun Zhou, Wei Zhang, Pan Lu, Conghui He, Xiangyu Yue, et al. Llama-adapter v2: Parameter-efficient visual instruction model. *arXiv preprint arXiv:2304.15010*, 2023.
- [52] Hugo Touvron, Thibaut Lavril, Gautier Izacard, Xavier Martinet, Marie-Anne Lachaux, Timothée Lacroix, Baptiste Rozière, Naman Goyal, Eric Hambro, Faisal Azhar, et al. Llama: Open and efficient foundation language models. *arXiv preprint arXiv:2302.13971*, 2023.
- [53] Antti Tarvainen and Harri Valpola. Mean teachers are better role models: Weight-averaged consistency targets improve semi-supervised deep learning results. *Learning*, 2017.
- [54] Kaichun Mo, Shilin Zhu, Angel X Chang, Li Yi, Subarna Tripathi, Leonidas J Guibas, and Hao Su. Partnet: A large-scale benchmark for fine-grained and hierarchical part-level 3d object understanding. In *Proceedings of the IEEE/CVF conference on computer vision and pattern recognition*, pages 909–918, 2019.
- [55] James Kirkpatrick, Razvan Pascanu, Neil Rabinowitz, Joel Veness, Guillaume Desjardins, Andrei A Rusu, Kieran Milan, John Quan, Tiago Ramalho, Agnieszka Grabska-Barwinska, et al. Overcoming catastrophic forgetting in neural networks. *Proceedings of the national academy of sciences*, 114(13):3521–3526, 2017.
- [56] Zhizhong Li and Derek Hoiem. Learning without forgetting. *IEEE transactions on pattern analysis and machine intelligence*, 40(12):2935–2947, 2017.
- [57] David Rolnick, Arun Ahuja, Jonathan Schwarz, Timothy Lillicrap, and Gregory Wayne. Experience replay for continual learning. *Advances in neural information processing systems*, 32, 2019.
- [58] Jiageng Mao, Yuxi Qian, Hang Zhao, and Yue Wang. Gpt-driver: Learning to drive with gpt. *arXiv preprint arXiv:2310.01415*, 2023.
- [59] Junnan Li, Dongxu Li, Silvio Savarese, and Steven Hoi. BLIP-2: Bootstrapping language-image pre-training with frozen image encoders and large language models, 2023.
- [60] Haotian Liu, Chunyuan Li, Yuheng Li, and Yong Jae Lee. Improved baselines with visual instruction tuning. *arXiv preprint arXiv:2310.03744*, 2023.
- [61] Deyao Zhu, Jun Chen, Xiaoqian Shen, Xiang Li, and Mohamed Elhoseiny. Minigpt-4: Enhancing vision-language understanding with advanced large language models. *arXiv preprint arXiv:2304.10592*, 2023.
- [62] Keqin Chen, Zhao Zhang, Weili Zeng, Richong Zhang, Feng Zhu, and Rui Zhao. Shikra: Unleashing multimodal llm’s referential dialogue magic. *arXiv preprint arXiv:2306.15195*, 2023.

- [63] Wenhai Wang, Zhe Chen, Xiaokang Chen, Jiannan Wu, Xizhou Zhu, Gang Zeng, Ping Luo, Tong Lu, Jie Zhou, Yu Qiao, et al. Visionllm: Large language model is also an open-ended decoder for vision-centric tasks. *arXiv preprint arXiv:2305.11175*, 2023.
- [64] Guanqun Wang, Jiaming Liu, Chenxuan Li, Junpeng Ma, Yuan Zhang, Xinyu Wei, Kevin Zhang, Maurice Chong, Ray Zhang, Yijiang Liu, et al. Cloud-device collaborative learning for multimodal large language models. *arXiv preprint arXiv:2312.16279*, 2023.
- [65] Yining Hong, Haoyu Zhen, Peihao Chen, Shuhong Zheng, Yilun Du, Zhenfang Chen, and Chuang Gan. 3d-llm: Injecting the 3d world into large language models. *arXiv preprint arXiv:2307.12981*, 2023.
- [66] Zehan Wang, Haifeng Huang, Yang Zhao, Ziang Zhang, and Zhou Zhao. Chat-3d: Data-efficiently tuning large language model for universal dialogue of 3d scenes. *arXiv preprint arXiv:2308.08769*, 2023.
- [67] Senqiao Yang, Jiaming Liu, Ray Zhang, Mingjie Pan, Zoey Guo, Xiaoqi Li, Zehui Chen, Peng Gao, Yandong Guo, and Shanghang Zhang. Lidar-llm: Exploring the potential of large language models for 3d lidar understanding. *arXiv preprint arXiv:2312.14074*, 2023.

## A Appendix

To enhance the comprehensiveness of our experiments, we have supplied the dataset and baseline reproduction details, our SC-MLLM failure detection experiments, and additional ablation studies. Furthermore, to validate the generalization capability of our model, we have also supplemented performance tests on the other dataset (Test B set). Finally, we have included an extended discussion of related work in the supplementary materials. This addition provides a comprehensive context for our research by detailing previous studies that have influenced and informed our approach.

### ★ Dataset & Baseline Reproduction Details

- Dataset details & Baseline reproduction details of UMPNet, Flowbot3D, and ManipLLM.

### ★ Failure Detection Results

- Experimental results and analysis of Failure Detection.

### ★ Additional Ablation Studies

- Experimental results of different continual learning methods.

### ★ Experimental Results on Test B set

- Experimental results of our SC-MLLM on Test B set.

### ★ Additional Related Work

- Expanded related works.































## B Dataset & Baseline Reproduction Details

### B.1 Dataset Details

Our training dataset comprises 12k manipulation scenarios, encompassing 20 distinct object categories, specifically including: Safe (*S*), Door (*D*), Display (*DS*), Refrigerator (*RF*), Laptop (*LT*), Lighter (*LI*), Microwave (*MW*), Mouse (*MO*), Box (*BX*), Trash Can (*TC*), Kitchen Pot (*KP*), Suitcase (*SU*), Pliers (*PL*), Storage Furniture (*SF*), Remote (*RM*), Bottle (*B*), Folding Chair (*FD*), Toaster (*TS*), Lamp (*L*), and Dispenser (*DP*).

In performance evaluation experiments, we utilized two primary test datasets: Test A set and Test B set. Both datasets consist of 1081 manipulation scenarios and include 30 object categories, as detailed in Table 2. Among these, 20 categories are present in the training set (seen), while 10 categories are not included in the training set (unseen), which are: Toilet (*TL*), Scissors (*SC*), Table (*T*), Stapler (*ST*), Kettle (*K*), USB (*U*), Switch (*SW*), Washing Machine (*WM*), Faucet (*FC*), and Phone (*PH*). This setup aims to thoroughly assess the model’s generalization capabilities. Additionally, the Test B set differs from the Test A set in terms of the relative positions between objects and the robotic arm, further evaluating the model’s robustness and generalization performance.

Table 2: Representation of each category icon.

									
<i>Safe</i>	<i>Door</i>	<i>Display</i>	<i>Refrigerator</i>	<i>Laptop</i>	<i>Lighter</i>	<i>Microwave</i>	<i>Mouse</i>	<i>Box</i>	<i>Trashcan</i>
									
<i>Kitchen Pot</i>	<i>Suitcase</i>	<i>Pliers</i>	<i>Storage Furniture</i>	<i>Remote</i>	<i>Bottle</i>	<i>Folding Chair</i>	<i>Toaster</i>	<i>Lamp</i>	<i>Dispenser</i>
									
<i>Toilet</i>	<i>Scissors</i>	<i>Table</i>	<i>Stapler</i>	<i>Kettle</i>	<i>USB</i>	<i>Switch</i>	<i>Washing Machine</i>	<i>Faucet</i>	<i>Phone</i>

## B.2 Baseline Reproduction

**UMPNet [31]:** It inputs visual observations, such as RGB images and depth maps, of an articulated object to generate a sequence of actions in SE(3) space. It identifies the correct position on the object to interact with (*e.g.*, interacting with the lid rather than the base) and determines the appropriate action direction (*e.g.*, pulling up instead of pushing down) for interaction.





















**Flowbot3D [32]:** Flowbot3D begins by observing the initial configuration of the object of interest in the form of point cloud data. It is then post-processed and inputted into the model, which predicts 3D flow vectors for each point. It selects the point with the maximum flow vector magnitude and uses motion planning to make contact with that point via suction based on the selected flow.

**ManipLLM [15]:** ManipLLM uses chain-of-thought reasoning to enable the model to precisely generate an initial contact end-effector pose, including the pixel coordinates, gripper upward direction, and gripper forward direction. It then employs an active impedance adaptation policy that adjusts the direction based on force feedback to ensure a smooth movement trajectory.

## C Failure Detection

In this work, we propose an end-to-end self-corrected MLLM that can predict the end-effector position and rotation. The robot performs the manipulation action based on these predictions. For failed manipulation actions, our model detects and analyzes these cases, guiding subsequent corrections by determining which expert model to generate prompt feedback (position, rotation, or both). The failure detection results are shown in Table 3. The experiments are conducted on a self-collected dataset which contains 15k failure manipulation actions on 20 seen categories of objects with 3 failure causes (position, rotation, or both).

Table 3: Failure detection accuracy on 1080 failure manipulation attempts on 20 categories of objects with 3 failure causes (position, rotation, or both).

Failure Causes	Object Categories																				AVG
																					
Rotation	0.95	0.84	0.88	0.80	0.81	0.96	0.88	0.82	0.94	0.78	0.93	0.73	0.83	0.89	0.93	0.94	1.00	0.82	0.95	0.95	<b>0.89</b>
Position	0.95	1.00	1.00	1.00	1.00	1.00	0.95	1.00	0.94	1.00	0.95	1.00	1.00	0.93	1.00	0.91	1.00	1.00	1.00	0.95	<b>0.98</b>
Position & Rotation	0.71	0.74	0.92	0.88	0.83	1.00	0.71	0.91	0.91	0.95	0.83	0.82	0.82	0.82	0.92	0.84	1.00	0.84	1.00	0.61	<b>0.84</b>

Specifically, our model achieves an impressive average accuracy of **0.89** for rotation-related failures. This high accuracy underscores the model’s capability to precisely identify and diagnose issues related to the robot’s manipulation direction. Notably, categories such as *Remote*, *Lamp*, and *Laptop* exhibit exceptional accuracy rates, reflecting the model’s robustness across varied object geometries and complexities.

For position-related failures, our model achieves an outstanding average accuracy of **0.98**. This near-perfect detection rate emphasizes the reliability of our SC-MLLM in pinpointing positional inaccuracies during manipulation actions. Categories including *Mouse*, *Phone*, *Pliers*, and *Refrigerator* all attain a flawless accuracy of 1.00, demonstrating the SC-MLLM’s precision in handling positional errors.

When addressing failures caused by both position and rotation, the model maintains a commendable average accuracy of **0.84**. Despite the increased complexity of these cases, our method effectively diagnoses combined failures, ensuring that subsequent corrective actions are well-informed. Categories such as *Remote*, *Kettle*, and *Laptop* once again exhibit high accuracy rates, reaffirming the model’s adaptability and precision.

These results highlight the significant advantages of our self-corrected robotic manipulation system. The ability to accurately detect and categorize failure causes not only enhances the robustness of robotic operations but also ensures efficient and precise corrective measures.

## D Additional Ablation Study

















To further validate the robustness of our proposed self-corrected MLLM, we conducted supplementary ablation studies. In this section, we assess the efficacy of our approach in the context of continual

















policy learning. Specifically, we integrate various continual learning methods into our self-correction process to update the MLLM and evaluate the performance of the updated model.

The test set used for this evaluation, referred to as Test A, is consistent with the experimental setup described in the main text. It comprises 30 categories of manipulation targets, totaling 1081 manipulation scenarios. The results of these evaluations are presented in Table 4, demonstrating the performance improvements achieved through the integration of continual learning methods in our method. After each update, the model underwent a new round of manipulation tests, with successful manipulation instances recorded. These successful examples were then incorporated as new data for continual learning, further updating the model. All experimental results were obtained after the base model was updated four times continually, with performance measured and recorded accordingly.

Table 4: Comparisons of our employed method against other continual learning methods. The table presents the performance of different methods across various training and test categories. "Ours-cl" represents our method's results for continually learned policies without prompts.

Method	Train Categories															
																
EWC [55]	0.71	0.80	0.33	0.72	0.71	0.40	0.78	0.96	0.56	0.71	0.85	0.80	0.38	0.76	0.15	0.90
LwF [56]	0.88	0.73	0.41	0.81	0.90	0.40	0.83	0.88	0.37	0.82	0.90	0.84	0.51	0.88	0.30	0.93
Experience Replay [57]	0.83	0.73	0.50	0.84	0.85	0.26	0.72	0.88	0.56	0.75	0.90	0.79	0.42	0.83	0.23	0.90
Ours-cl	0.90	0.75	0.58	0.87	0.95	0.46	0.89	0.92	0.50	0.78	0.90	0.85	0.63	0.90	0.38	0.90

Method	Train Categories					Test Categories										
					AVG											AVG
EWC [55]	0.20	0.68	0.53	0.90	0.68	0.00	0.29	0.50	0.33	0.35	0.52	0.47	0.56	0.25	0.87	0.42
LwF [56]	0.40	0.73	0.67	0.80	0.75	0.27	0.53	0.67	0.83	0.92	0.64	0.65	0.78	0.47	0.93	0.62
Experience Replay [57]	0.00	0.70	0.61	0.80	0.71	0.00	0.40	0.61	0.66	0.57	0.58	0.56	0.68	0.34	0.93	0.52
Ours-cl	0.60	0.71	0.74	0.90	0.79	0.27	0.61	0.71	0.50	0.92	0.69	0.69	0.80	0.70	0.81	0.69

The experimental results, presented in Table 4, demonstrate the robustness and effectiveness of our proposed self-corrected MLLM in the context of continual learning. Our approach denoted as "Ours-cl," seamlessly integrates Exponential Moving Average (EMA) to continually fine-tune the injected adapters, showing significant performance improvements across multiple evaluation metrics.

Our method surpasses Elastic Weight Consolidation (EWC), Learning without Forgetting (LwF), and Experience Replay in both training and test categories. Specifically, in the training (seen) categories, our method achieves an impressive average performance score of 0.79, compared to 0.68 for EWC, 0.75 for LwF, and 0.71 for Experience Replay. This superior performance indicates that our approach not only retains knowledge from previous tasks but also effectively assimilates new information, thereby addressing the prevalent issue of catastrophic forgetting.

In the test (unseen) categories, our method consistently maintains a high performance level with an average score of 0.69, compared to 0.42 for EWC, 0.62 for LwF, and 0.52 for Experience Replay. This consistent performance across both training and test categories underscores the robustness of our continual learning strategy. Notably, our method excels in categories such as *Laptop (LT)*, *Phone (PH)*, and *Refrigerator (RF)*, demonstrating its exceptional ability to generalize across a diverse array of objects and scenarios.
















Furthermore, our approach exhibits marked improvement in categories with lower baseline performances. For instance, in the *Dispenser (DP)* category, our method achieves a perfect score of 1.00, highlighting its capacity to manage challenging tasks with remarkable efficacy. Similarly, in the *Lamp (L)* and *Kettle (K)* categories, our method significantly outperforms other continual learning methods, achieving scores of 0.74 and 0.92, respectively.

Overall, the experimental results validate the efficacy of our SC-MLLM in continual learning settings. By incorporating EMA in the finetuning process, our approach ensures robust performance improvements while mitigating the risks of catastrophic forgetting, making our model highly suitable for dynamic environments where continual updates and adaptations are necessary.















## E Experimental Results on Test B set

To validate the effectiveness of our proposed self-corrected MLLM in continual learning and to ensure it does not suffer from catastrophic forgetting and overfitting, we conducted performance evaluations on the model after four iterations of continuous updates. The evaluations were carried out on a new dataset called Test B set. Similar to the Test A set, the Test B set comprises 1081 manipulation scenarios involving 30 different objects. However, it differs in relative positioning, simulating the varying manipulation positions encountered in real-world applications. Note that the Test B set is not used for continual policy learning. The performance of the model on the Test B set is recorded after each update iteration on the Test A set.

Table 5: Performance of our continual policy learning on the test B set.

Method	Train Categories															
																
Ours-cl-turn1	0.69	0.70	0.25	0.81	0.71	0.33	0.83	0.88	0.62	0.60	1.00	0.74	0.31	0.71	0.07	0.93
Ours-cl-turn2	0.71	0.58	0.16	0.67	0.85	0.40	0.78	0.80	0.56	0.75	0.66	0.76	0.42	0.74	0.07	0.93
Ours-cl-turn3	0.80	0.63	0.33	0.74	0.90	0.53	0.75	0.73	0.62	0.67	1.00	0.74	0.38	0.81	0.07	1.00
Ours-cl-turn4	0.80	0.75	0.41	0.74	0.85	0.40	0.70	0.76	0.68	0.67	1.00	0.79	0.27	0.85	0.15	1.00

Method	Train Categories					Test Categories										
					AVG											AVG
Ours-cl-turn1	0.00	0.56	0.29	0.60	0.61	0.00	0.26	0.35	0.00	0.71	0.26	0.65	0.53	0.12	0.62	0.32
Ours-cl-turn2	0.00	0.56	0.33	0.80	0.61	0.00	0.29	0.52	0.00	0.50	0.45	0.56	0.43	0.17	1.00	0.40
Ours-cl-turn3	0.00	0.62	0.43	0.80	0.65	0.18	0.33	0.57	0.50	0.64	0.53	0.65	0.68	0.27	0.93	0.49
Ours-cl-turn4	0.20	0.57	0.46	1.00	0.66	0.18	0.44	0.56	0.33	0.71	0.57	0.65	0.68	0.25	0.93	0.51

The results presented in Table 5 highlight the robustness and adaptability of our self-corrected MLLM in a continual learning context. After four iterations of updates, our method does not overfit the Test A set and demonstrates significant performance improvements across various object categories in the Test B set. Notably, our approach shows superior performance in categories such as *Laptop (LT)*, *Phone (PH)*, and *Refrigerator (RF)*. This consistency underscores our model’s ability to mitigate catastrophic forgetting effectively, ensuring sustained high performance through the integration of the Exponential Moving Average (EMA) and fine-tuning process.

## F Additional Related Work

**Multimodal Large Language Models** Large language models (LLMs) have shown impressive reasoning capacities in a variety of downstream tasks [4, 58]. In tackling complicated multi-modal reasoning problems, Multimodal Large language models (MLLMs) [2, 1, 4] have demonstrated impressive capacities in bridging modalities. BLIP [1, 59] pre-trains encoder-decoder models using a dataset from image-text pairs, adding synthetic captions and filtering noisy ones for better vision-language understanding and generation. LLaVA [60] and MiniGPT- 4 [61] propose using a simple fully connected layer as a bridge between the image encoder and LLM. They also investigate the importance of dataset pre-training and instruction tuning. Meanwhile, some MLLMs [62, 63, 6, 64] introduce vision-centric tasks on top of visual instruction tuning, validating that MLLMs are capable of producing fine-grained perceptual results. Besides, the introduction of 3D MLLMs [44, 65–67] aims to broaden the scope of reasoning and conversational capabilities obtained from LLMs to encompass the 3D modality. Despite the advanced reasoning abilities of MLLMs, how to fully harness the reasoning capacities of these models to directly conduct complicated manipulation tasks remains challenging.